Rock and Soil Mechanics

Volume 43 | Issue 4 Article 6

6-9-2022

Microstructure variation and empirical fatigue model of salt rock under cyclic loading

Qiang ZHANG
Shaanxi Key Laboratory of Geotechnical and Underground Space Engineering, Xi'an University of Architecture and Technology, Xi'an, Shaanxi 710055, China

Jun-bao WANG
Shaanxi Key Laboratory of Geotechnical and Underground Space Engineering, Xi'an University of Architecture and Technology, Xi'an, Shaanxi 710055, China

Zhan-ping SONG
Shaanxi Key Laboratory of Geotechnical and Underground Space Engineering, Xi'an University of Architecture and Technology, Xi'an, Shaanxi 710055, China

Shi-jin FENG
Department of Geotechnical Engineering, Tongji University, Shanghai 200092, China

See next page for additional authors

Custom Citation

ZHANG Qiang, WANG Jun-bao, SONG Zhan-ping, FENG Shi-jin, ZHANG Yu-wei, ZENG Tao, . Microstructure variation and empirical fatigue model of salt rock under cyclic loading[J]. Rock and Soil Mechanics, 2022, 43(4): 995-1008.

Microstructure variation and empirical fatigue model of salt rock under cyclic loading

Authors

Qiang ZHANG, Jun-bao WANG, Zhan-ping SONG, Shi-jin FENG, Yu-wei ZHANG, and Tao ZENG

Rock and Soil Mechanics 2022 43(4): 995−1008 ISSN 1000−7598
https: //doi.org/10.16285/j.rsm.2021.6356 rocksoilmech.researchcommons.org/journal

Microstructure variation and empirical fatigue model of salt rock under cyclic loading

ZHANG Qiang[1, 2], WANG Jun-bao[1, 2], SONG Zhan-ping[1, 2], FENG Shi-jin[3], ZHANG Yu-wei[1, 2], ZENG Tao[1, 2]

1. School of Civil Engineering, Xi'an University of Architecture and Technology, Xi'an, Shaanxi 710055, China
2. Shaanxi Key Laboratory of Geotechnical and Underground Space Engineering, Xi'an University of Architecture and Technology, Xi'an, Shaanxi 710055, China
3. Department of Geotechnical Engineering, Tongji University, Shanghai 200092, China

Abstract: To study the fatigue properties and microstructure variation of salt rock under cyclic loading, uniaxial fatigue tests under different maximum cycling stresses were carried out on salt rock specimens. Meanwhile, scanning electron microscopy (SEM) and nuclear magnetic resonance (NMR) instruments were utilized to analyze the microstructure variation in salt rock before and after the test. The results indicated that the cracks growth mode in salt rock under cyclic loading is mainly the development of intergranular cracks, and the number of cracks increases with the maximum stress ratio (the ratio of the maximum cycling stress to the uniaxial compressive strength). After cyclic loading (12 000 cycles), the number of large pores and total pores in salt rock both increase, whereas the number of small pores decreases; and with the increase of maximum stress ratio, the increasing number of large pores and total pores and the decreasing number of small pores both increase. When the maximum stress ratio is 0.40 and the cycle number $N \leqslant 2\,000$, the numbers of small pores, large pores and total pores all increase with cycle number; but the increase rate of small pores is faster than that of large pores, showing that the pore structure variation in salt rock is dominated by the initiation of small pores. When the maximum stress ratio is 0.40 and the cycle number $N > 2\,000$, the number of large pores and total pores still increase with cycle number, whereas the number of small pores decreases, demonstrating that the formation of large pores accounts for the main change of pore structure. By solving the inverse function of S-shaped function, an empirical fatigue model with simpler form and fewer parameters was established, which can describe the whole process of irreversible deformation development of salt rock with a unified function, and the rationality of the model was verified by the fatigue test results of salt rock.

Keywords: salt rock; cyclic loading; microstructure; SEM; NMR; empirical fatigue model

1 Introduction

Salt rock possesses many advantages, such as compact structure, low permeability, stable mechanical properties and strong damage self-healing ability, and thus is regarded as an ideal medium for constructing underground salt cavern gas storage and compressed air energy storage (CAES) station[1−2]. The operation procedure of salt cavern gas storage and CAES station includes four stages: gas injection and pressurization, high-pressure operation, gas recovery and depressurization, and low-pressure operation, as shown in Fig. 1. In the gas injection and pressurization stage, the pressure in the storage gradually increases, and the unbalance force of the surrounding rock around the cavern decreases gradually. In the high-pressure operation stage, the pressure in the storage is maintained at a high level and basically unchanged, and the unbalance force of the rock around the cavern is small and relatively constant. In the gas recovery and depressurization stage, the pressure in the storage pressure gradually decreases, and the unbalance force of the rock around the cavern gradually increases. In the low-pressure operation stage, the internal pressure remains at a low level and basically unchanged, while the unbalance force of the surrounding rock is large and relatively constant. Due to the periodic gas injection and production, surrounding rock will withstand cyclic loading in the long-term operation of salt cavern gas storage and CAES station[3]. Therefore, in order to ensure the long-term safety and stability of underground salt cavern gas storage and CAES station, it is of great significance to study the fatigue characteristics of salt rock under cyclic loading[4−5].

Received: 16 August 2021 Revised: 8 November 2021
This work was supported by the National Natural Science Foundation of China (52178393, 52178354), the Housing and Urban-Rural Construction Science and Technology Planning Project of Shaanxi Province (2019-K39), the China Postdoctoral Science Foundation (2018M643809XB), the Natural Science Basic Research Program of Shaanxi Province (2019JQ-762) and the Innovation Capability Support Plan of Shaanxi - Innovation Team (2020TD-005).
First author: ZHANG Qiang, male, born in 1989, PhD. candidate, mainly engaged in research of rock mechanics and underground engineering. E-mail: nndsjyzq@163.com
Corresponding author: WANG Jun-bao, male, born in 1982, PhD, Professor, mainly engaged in the teaching and research of rock mechanics and underground engineering. E-mail: xajdwangjunbao@163.com

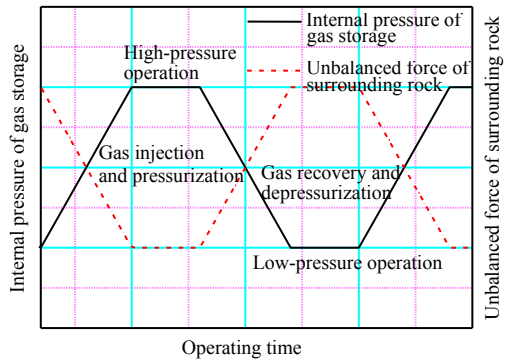

Fig. 1 Variation of internal pressure and unbalanced force of surrounding rock for salt cavern storage

Since salt rock plays an important role in the underground storage of natural gas and other energy sources, scholars have studied the fatigue properties of salt rock from different perspectives. Ma et al. studied the effects of stress amplitude, loading frequency, maximum and minimum cycling stress on the strength, deformation and damage characteristics of salt rock[6]. Guo et al. found that with the increase of the average stress or maximum stress ratio of cyclic loading, the fatigue process of salt rock is significantly shortened and the total deformation caused by fatigue failure is substantially reduced [7]. On the basis of summarizing the fatigue test results of salt rock at different temperatures, Ren et al. discussed the influence of temperature on the development of internal damage and fatigue life of salt rock[8]. Pouya et al. analyzed the influence of cyclic loading on the damage development of salt rock by connecting the micro stress, macro stress, micro viscoplastic strain and macro viscoplastic strain together and using the inclusion matrix model[9]. Fan et al. carried out fatigue tests on salt rock with intermittent time, and pointed out that with the extension of intermittent time, the internal damage of salt rock gradually increases and the fatigue life gradually shortens[10]. Jiang et al. explained the damage mechanism of salt rock under cyclic loading with intermittent time from a theoretical perspective, and stated that the Bauschinger effect and residual stress are the main reasons for shortening the fatigue life of salt rock[11]. Although there are many investigations on fatigue properties of salt rock, most of them focus on the influence of cyclic loading on the macroscopic mechanical parameters (such as strength and deformation), and few on the influence of microstructure. In fact, the deterioration of mechanical properties of salt rock under cyclic loading is the macro performance of its internal damage accumulation. Therefore, microscopic studies on the internal structural changes of salt rock under cyclic loading is of great value to correctly understand the fatigue mechanism of salt rock[12−14].

In order to quantitatively describe the development law of rock irreversible deformation, numerous fatigue constitutive models have been constructed by combining laboratory fatigue tests and analytical solutions. In general, these models can be divided into two categories:

(1) Damage fatigue model. Li et al. set up a rock low-cycle fatigue damage model combining the continuum damage mechanics theory from the viewpoint of mechanical deterioration of rock under cyclic loading[15]. Wang et al. proposed a low-cycle damage model for salt rock considering the effects of loading frequency and stress amplitude based on fatigue test results and the Manson−Coffin equation[16]. On the basis of analyzing the variation of residual strain and elastic modulus of fractured rock with loading cycles, Li et al. constructed a damage model of fractured rock mass from the perspective of energy dissipation[17]. Liu et al. established the damage evolution equation under cyclic loading based on energy dissipation, and established the rock fatigue damage constitutive model by recursive method[18]. Although the damage fatigue constitutive model can effectively reflect the fatigue characteristics of rock under cyclic loading, it is difficult to select reasonable damage variables to characterize the damage evolution[19].

(2) Element combined fatigue model. In recent years, due to the similarity between cumulative irreversible deformation curve and creep curve, scholars have set about building rock fatigue constitutive model by referring to the results of element combined creep model. Guo et al. proposed three basic fatigue elements, and built a constitutive model reflecting rock fatigue deformation behavior based on the Burgers creep model[20]. Peng et al.[21] proposed joint plastic and viscous fatigue elements based on the analysis of rock fatigue characteristic curves, and constructed a constitutive model describing the viscoelastic-plastic fatigue deformation behavior of jointed rock in combination with the research of literature [20]. Li et al. replaced the viscosity element in Nishihara model with nonlinear element containing fatigue parameters, and constructed an improved Nishihara model describing three stages of rock fatigue deformation[22]. Tang et al. used the Murayama visco-elastomer with switch function to replace the Kelvin element in Nishihara model, and used the nonlinear viscous element with fatigue parameters to replace the linear element in the viscoplastic element, so as to build a constitutive model characterizing the rock deformation under cyclic loading[23]. Liu et al. proposed three-dimensional viscous, elastic and plastic fatigue elements and rock fatigue yield criteria under cyclic loading, and then constructed a three-dimensional viscoelastic-plastic fatigue model[24]. However, when

the element combined model is applied to describe the rock fatigue deformation, the original continuous fatigue deformation needs to be artificially divided into three stages (initial stage, constant stage and acceleration stage), and different functions are required to describe the fatigue deformation behavior at an individual stage. Meanwhile, it is inconvenient to apply these rock fatigue constitutive models since most of them evolve complex forms and many parameters[25].

In this study, the uniaxial fatigue tests of salt rock under different maximum cycling stress (constant minimum cycling stress and loading frequency) are carried out in the laboratory. Meanwhile, the microstructure of salt rock before and after the tests is systematically observed by scanning electron microscopy (SEM) and nuclear magnetic resonance (NMR) system. Based on the test results, the variation law of micropore structure of salt rock with maximum cycling stress and cycle numbers is analyzed. On this basis, an empirical fatigue model is provided by solving the inverse function of S-shaped function, and the rationality of the model is verified by using the fatigue test results.

2 Uniaxial fatigue test

2.1 Specimen preparation

The rock specimens in this test were taken from a salt mine in Pakistan at a depth of about 600 m. The specimens are light red or white, mainly composed of NaCl (≥98%), and a small amount of K_2SO_4、Na_2SO_4 and argillaceous insoluble matter. As salt rock is easy to dissolve in water, the specimens were processed into standard cylinders with diameter ratio of 1:2 (50 mm in diameter and 100 mm in height) by using dry grinding method in the dry environment. In addition, in order to prevent deliquescence of salt rock due to moisture absorption in the air during storage, the processed specimens were wrapped with plastic wraps, as shown in Fig. 2.

Fig. 2 Salt rock specimens

2.2 Test equipment

This research aims at studying the effects of maximum cycling stress on fatigue characteristics and microstructure of salt rock. Uniaxial fatigue tests of salt rock under different maximum cycling stresses were carried out in the laboratory, and the microstructure of salt rock before and after fatigue was observed by SEM and NMR. The main devices used in this test are:

(1) Electro-hydraulic servo fatigue testing machine: the maximum axial load and the maximum axial displacement that can be applied by the equipment are 250 kN and 75 mm, the measurement accuracy of which are within ±0.5%, and the displacement resolution is 0.001 mm. The loading waveform includes triangle wave, square wave and sine wave.

(2) Quanta 200 SEM: The device has a maximum resolution of 3.5 nm and a maximum effective magnification of 1 000 000.

(3) MacroMR 12-150H-I NMR system: The magnetic field intensity is 0.3±0.05 T, the magnetic field uniformity is 35×10^{-6}, the peak output is more than 300 W, the linear distortion is less than 0.5%, and the effective sample detection range is ϕ150 mm×H100 mm.

2.3 Test scheme

Before the fatigue test, the basic physical and mechanical properties of salt rock were tested, as listed in Table 1.

Table 1 Basic physical and mechanical parameters of salt rock

Density /(g • cm^{-3})	UCS (Uniaxial compressive strength) /MPa	Elastic modulus /GPa	Poisson's ratio
2.21	35.18	15.33	0.29

Note: The data in Table 1 are the mean values.

In the long-term operation of salt cavern gas storage and CAES station, the loading waveform acting on the surrounding rock around the cavern is trapezoidal wave, as shown in the dotted line in Fig. 1. Given that the strata unbalance force is basically unchanged in the high-pressure and low-pressure operation stages, the surrounding rock only produces creep deformation, rather fatigue deformation. Hence, triangle wave is used as stress loading waveform to perform salt rock fatigue test in this study, as illustrated in Fig. 3.

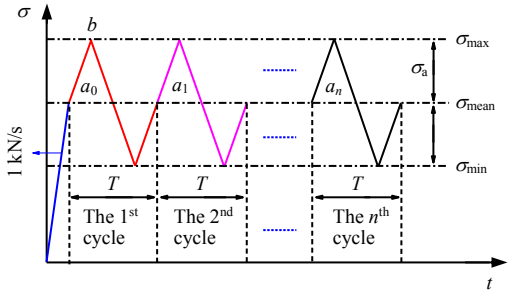

Fig. 3 Sketch map of stress loading waveform

The buried depth of the specimens is about 600 m. According to the Hoek and Brown's statistical law[26], the corresponding vertical in-situ stress is 16.20 MPa. The maximum and minimum storage pressures of underground salt cavern storage are generally 70% and 20% of the overburden formation pressure[27]. For the buried depth of salt rock used in this paper, if the maximum storage pressure is 70% of the overburden formation pressure, the unbalance force is 30% of the overburden formation pressure, which is 4.86 MPa. Therefore, the minimum cycling stress selected is 5 MPa, and the corresponding ratio of minimum stress R_L (the ratio of minimum cycling stress to uniaxial compressive strength) is assumed as 0.14. In addition, the research objective is the influence of maximum cycling stress on fatigue characteristics and microstructure in this paper. For this purpose, uniaxial fatigue tests at 8, 14, 20, 23, 26 and 30 MPa have been conducted on six salt rock specimens. The corresponding ratio of maximum stress R_H (the ratio of maximum cycling stress to uniaxial compressive strength) is 0.23, 0.40, 0.57, 0.65, 0.74 and 0.85.

For salt cavern CAES station, it usually experiences one gas injection and recovery cycle in a day. According to the calculation, the number of load cycles experienced by the surrounding rock can reach 11 000 times in its designed service life (30 a). In order to ensure that the specimens experience enough the number of load cycles and minimize the influence of creep on fatigue test, the maximum load cycle was set as 12 000 times and the load frequency was 1 Hz. Under this setting, a fatigue test can be completed within 3.4 h. Zhao et al.[28], Guo et al.[7] also confirmed that under such test conditions, the creep deformation of salt rock is insignificant due to the short test period, and the influence of creep on fatigue test results can be ignored.

2.4 Test procedure

The test procedure includes the following steps: (1) Weigh the initial mass of the specimen m_0, and then perform vacuum saturation in saturated brine. Weigh the mass of the specimen every 4 h until the mass difference between adjacent two times is less than 0.01 g. (2) NMR system is used to test the micro pores of saturated specimens. (3) Place the specimens in a constant temperature oven at 40 ℃ and weigh them every 2 h until the mass difference between adjacent two times is less than 0.01 g. (4) Install the specimens on the fatigue test machine. (5) Apply axial stress at a rate of 1 kN/s to the mean value of cyclic loading (point a_0 in Fig. 2). (6) Take a_0 point as the starting point, apply cyclic loading repeatedly until the failure of the specimens or the cycle number reaches 12 000 times and then stop the test. (7) For the intact specimens, NMR test is carried out after resaturation treatment. The test process is the same as steps (1) and (2). (8) Detect the microstructure of the specimens using SEM. Meanwhile, another three specimens without cyclic loading are selected to test their initial microstructure using SEM.

In addition, in order to study the variation of small pores structure of salt rock with cycle numbers, NMR is reapplied to observe another specimen (#7: R_H and R_L are 0.40 and 0.14, respectively, and the load frequency is 1 Hz) after 0, 500, 2 000, 5 000, 8 000 and 12 000 cycles. The test steps are the same as steps (1) to (7).

3 Fatigue test results analysis

3.1 Axial stress−strain curve

Figure 4 exhibits the axial stress−strain curves of specimens #1 to #6. It is found that: (1) When the maximum stress ratio is lower than 0.74, specimens #1 to #4 do not fail even after 12 000 cycles, and the axial stress−strain curves only contain two stages of “sparse to dense”. At the end of the test, the maximum axial strains of the four specimens are 0.51%, 1.01%, 1.96% and 2.74%. (2) When the maximum stress ratio is 0.74 and 0.85, the specimens #5 and #6 undergo 4 982 and 1 613 cycles respectively, and the axial stress-strain curves contain three stages of “sparse-dense-sparse”. At the end of the test, the maximum axial strains of the two specimens are 4.98% and 6.10%.

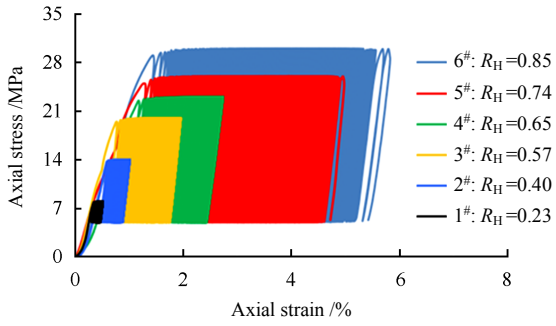

Fig. 4 Axial stress−strain curves of salt rock

3.2 Irreversible deformation

Under cyclic loading, the total deformation of rock in the loading stage is composed of elastic deformation and plastic deformation. The elastic deformation is completely recovered in the unloading stage, while the plastic deformation (irreversible deformation) will remain. Fig. 5 presents the variation of cumulative irreversible deformation of salt rock ε with the cycle numbers N. It is found that:

(1) When the maximum stress ratio is 0.74 and 0.85, fatigue failure occurs in specimens #5 and #6. The change of cumulative irreversible deformation

includes three stages: initial stage (cumulative irreversible deformation rate decreases gradually), constant rate stage (cumulative irreversible deformation rate keeps steady) and acceleration stage (cumulative irreversible deformation rate increases gradually).

(2) When the maximum stress ratio is lower than 0.74, no fatigue failure occurs in specimens #1 to #4. The changes of cumulative irreversible deformation only include initial and constant rate stages.

(3) The cumulative irreversible deformation of salt rock increases with the increase of maximum stress ratio when the cycle numbers remain the same.

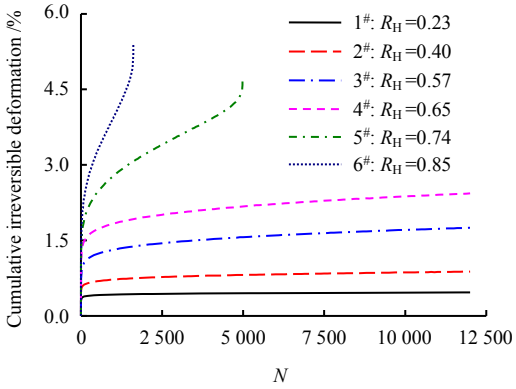

Fig. 5 Variation of cumulative irreversible deformation of salt rock with cycle numbers

4 SEM results analysis

The basic principle of scanning electron microscope (SEM) is that the electron beam emitted by high-voltage electron gun will produce various physical information after contacting with the surface of the observed material, and then collect, convert, adjust and reimage these information, and finally reflect the microstructure and morphology of the material in the form of image. The microstructure and cracks propagation mechanism of salt rock can be intuitively understood by analyzing SEM images of salt rock under cyclic loading.

4.1 SEM images of salt rock in the initial state

Figure 6 displays the SEM images of salt rock (2000×) in the initial state. The compact microstructure and close contact between grains are observed. No obvious pores and fissures are found even at a magnification of 2 000, suggesting the outstanding performance of salt rock such as low porosity, low permeability and good tightness. In addition, Fig. 6(d) highlights that grain size of salt rock vary greatly, and the contact surfaces between grains are extremely irregular. These irregular intergranular contact surfaces are likely to crack under the action of external loading, resulting in intergranular cracks.

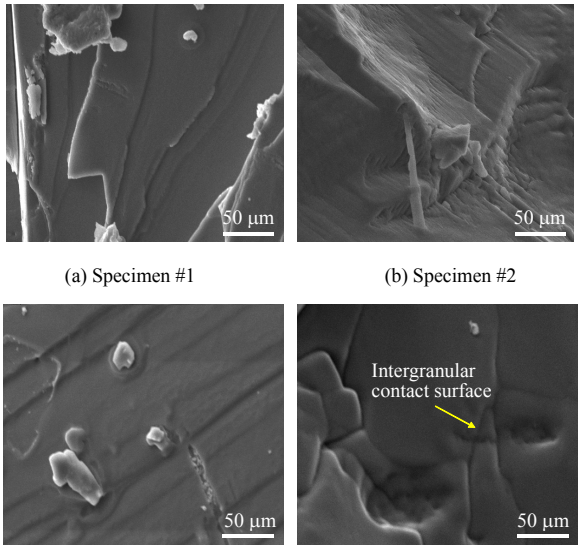

(a) Specimen #1 (b) Specimen #2

(c) Specimen #3 (d) Specimen #4

Fig. 6 SEM images of salt rock in initial state

4.2 SEM images of salt rock after cyclic loading

There are three modes of microcrack propagation in salt rock under external loading, namely the microcracks between the contact surfaces of salt rock grains (intergranular cracks), the microcracks cutting through salt rock grains (transgranular cracks) and the microcracks constrained within salt rock grains (intragranular cracks). Fig. 7 shows the salt rock SEM images (500×) after cyclic loading.

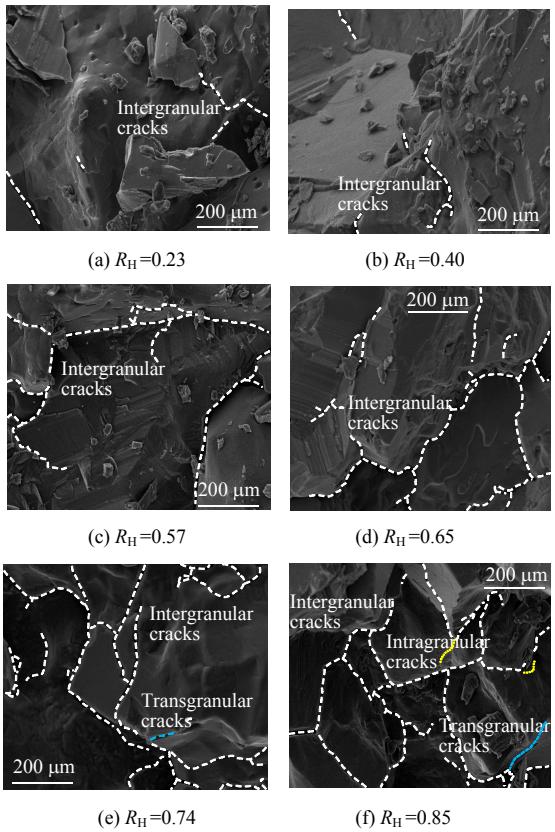

(a) R_H=0.23 (b) R_H=0.40

(c) R_H=0.57 (d) R_H=0.65

(e) R_H=0.74 (f) R_H=0.85

Fig. 7 SEM images of salt rock after cyclic loading

As illustrated in Fig. 7, the microstructure of salt rock changes significantly after cyclic loading compared with that in the initial state (Fig. 6). In general, the internal microstructure of salt rock is mainly characterized by intergranular cracks, and the number of cracks increases with the increase of maximum stress ratio R_H. In addition, when R_H is 0.74 and 0.85, a small quantity of transgranular cracks and intragranular cracks appear (as shown in Fig.7 (e) and 7(f)). For pure salt rock, its internal structure is microscopically characterized as a random material polymer with grains as units, and there are cleavage planes between grains that are easy to split. These cleavage planes are likely to crack under external loading, which explains that intergranular cracks dominate the internal cracks in salt rock under cyclic loading[29].

5 NMR result analysis

For saturated rock, pore radius r can be estimated from the transverse relaxation time T_2 obtained by NMR test:

$$r = \rho_0 F_s T_2 \quad (1)$$

where ρ_0 is the surface relaxation strength (μm/s); F_s is the pore shape coefficient (for cylindrical pores, F_s =2; for spherical pores, F_s =3). The transverse relaxation time T_2 is proportional to the pore radius. The larger T_2 is, the larger the pore radius is, and vice versa. According to the research of Tang et al.[30] and Yang et al.[31], pores corresponding to transverse relaxation time $T_2 \leqslant 10$ ms are identified as small pores in this paper, and those corresponding to T_2>10 ms are large pores.

5.1 T_2 spectrum distribution and area change under different maximum stress ratio

5.1.1 T_2 spectrum distribution

Since the transverse relaxation time is directly proportional to the pore radius (Eq. (1)), the variation of pore size in salt rock under cyclic loading can be intuitively characterized by analyzing the T_2 spectrum distribution before and after the test. Due to the fatigue failure of specimens #5 and #6, Fig. 8 only displays the T_2 spectrum of #1 to #4. As can be seen:

(1) Due to the discreteness among the specimens, the NMR parameters of the four specimens, such as the quantity of wave peaks, peak signal amplitude, and initial and final relaxation time, are different.

(2) Before the fatigue test, for specimens #1 (R_H = 0.23) and #2 (R_H =0.40), the minimum relaxation time corresponding to the first T_2 peak is 0.020 0 and 0.261 3 ms respectively. After the test, the minimum relaxation time corresponding to the first peak is 0.017 4 and 0.018 7 ms respectively. The leftward shifting first peak indicates that the cyclic loading causes the formation

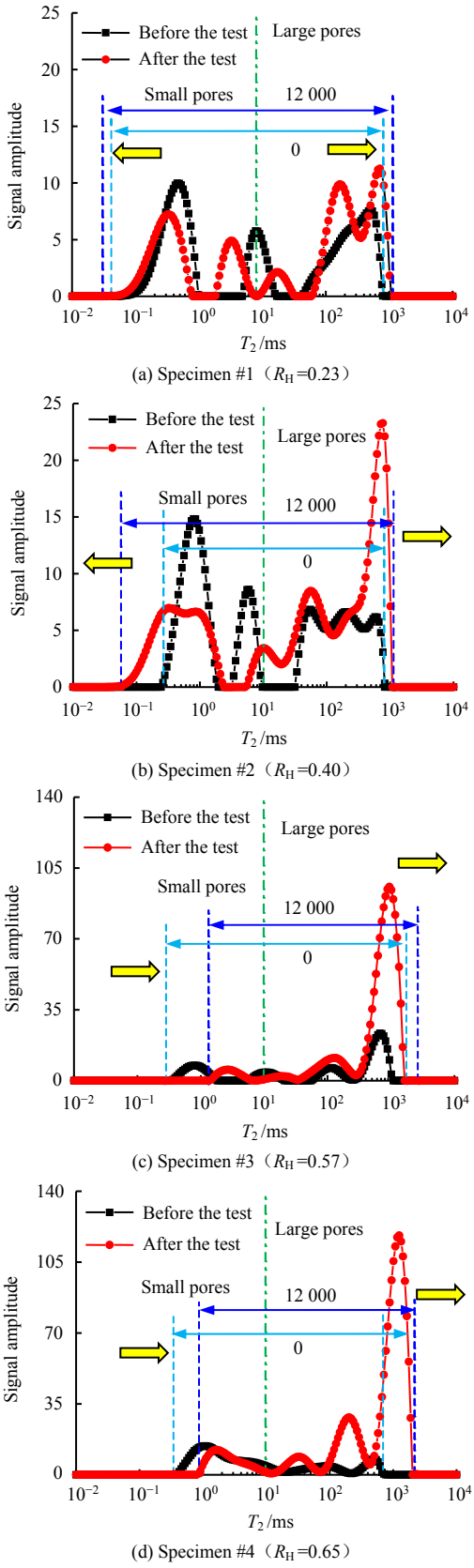

(a) Specimen #1（R_H=0.23）

(b) Specimen #2（R_H=0.40）

(c) Specimen #3（R_H=0.57）

(d) Specimen #4（R_H=0.65）

Fig. 8 T_2 spectrum distribution of salt rock before and after the test

of smaller pores in salt rock. The maximum relaxation time corresponding to the last T_2 peak is 766.341 (#1) and 821.434 4 ms (#2) before the test, and 1 011.638 0 ms (#1) and 1 162.322 5 ms (#2) after the test. The T_2

peaks of the two specimens shift to the right after the test, indicating that the pores are continuously connected to form large pores.

(3) Before the fatigue test, for specimens #3 (R_H= 0.57) and #4 (R_H=0.65), the minimum T_2 corresponding to the first peak of is 0.369 7 ms and 0.396 3 ms. After the test, the minimum T_2 corresponding to the first peak is 2.409 4 ms and 0.911 6 ms, showing that the first T_2 peaks of the two specimens move to the right. At this time, the change of pore size in salt rock is manifested in two ways: on the one hand, the cyclic loading causes the formation of new smaller pores in salt rock; on the other hand, under the cyclic loading of higher maximum stress ratio, these newly formed small pores and existing small pores with smaller size gradually coalesce to form small pores with larger size, which leads to the disappearance of original small pores. The maximum T_2 corresponding to the last peak is 1 011.638 0 ms (#3) and 666.992 0 ms (#4) before the test, and 2 494.508 1 ms (#3) and 1 889.652 3 ms (#4) after the test, respectively. The T_2 peaks of the two specimens shift to the right, indicating a tendency that small pores develop into large pores under cyclic loading. Simultaneously, the expansion of internal pores of specimens #3 and #4 is highly enhanced due to the larger maximum stress ratio, and thus #3 and #4 have larger maximum pore size than those of specimens #1 and #2.

5.1.2 T_2 spectrum area change

It has been proven that T_2 spectrum area is proportional to the quantity of pores, that is, a larger T_2 spectrum area represents more pores in the rock. Therefore, the influence of cyclic loading on the number of pores in salt rock can be quantitatively analyzed by comparing the T_2 spectrum area before and after the test. Table 2 compares the T_2 spectrum area distribution of specimens #1 to #4 before and after the test. It can be seen that:

(1) Although there are some differences in the T_2 peak number and signal amplitude of specimens #1 to #4 before the test, the total areas of T_2 spectrum are all within the range of 422.73 to 586.76, indicating that the difference of original pores in the four specimens is insignificant. In addition, except for specimen #3 (the spectrum area of small pores makes up 72.02% of the total area), the number of original small pores is more than that of large pores (the spectrum area of small pores accounts for more than 52% of the total area).

(2) After 12 000 loading cycles, the number of small pores in specimens #1 to #4 decreases to some extent. With the increase of maximum stress ratio, the number of small pores shows an upward trend. After the test, the corresponding areas of small pores decrease by 25.15, 62.38, 63.16 and 150.88. It shows that the newly formed small pores and existing small pores in salt rock are gradually connected into large pores under cyclic loading, and the larger the maximum stress ratio is, the more the number of small pores is connected. However, due to the discreteness of specimens and the dynamic and random changes in the amount of small pores, the reduction of small pores in specimens #2 and #3 is similar after the test.

(3) After 12 000 cycles, both the total pores and large pores in specimens #1 to #4 increase. The larger the maximum stress ratio is, the more the number of the total pores and large pores increase. The total T_2 spectrum areas increase by 79.78, 194.78, 1 061.21 and 1 606.01, and the corresponding large pores areas increase by 104.93, 261.16, 1 117.37 and 1 756.89. It is mainly reasons that the increase of maximum stress ratio leads to more newly formed pores in salt rock. Moreover, the number of large pores formed by the connection between new small pores and existing pores increases, and the total pores increase as well.

Table 2 Area distribution of T_2 spectrum for salt rock under different maximum stress ratios

Specimen	R_H	Test stage	Total area	Small pores		Large pores	
				Area	Ratio / %	Area	Ratio / %
#1	0.23	Before	422.73	221.36	52.36	201.37	47.64
		After	502.51	196.21	39.05	306.30	60.95
#2	0.40	Before	582.31	322.32	55.35	257.99	44.65
		After	777.09	259.94	33.45	519.15	66.55
#3	0.57	Before	489.16	136.85	27.98	359.31	72.02
		After	1 550.37	73.69	4.75	1 476.68	95.25
#4	0.65	Before	586.76	396.49	67.57	190.27	32.43
		After	2 192.77	245.61	11.20	1 947.16	88.80

Figure 9 describes the variation of total area increment ΔS of T_2 spectrum with maximum stress ratio of specimens #1# to #4.

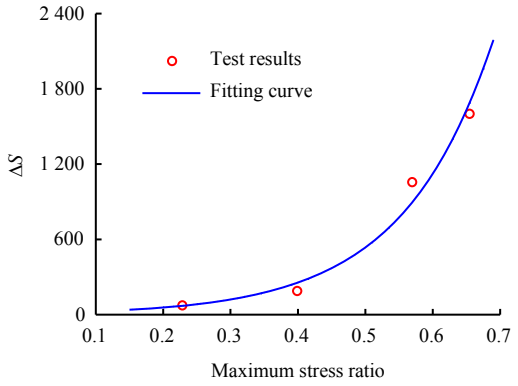

Fig. 9 Variation of total area increment of T_2 spectrum with maximum stress ratio

As illustrated in Fig. 9, when the maximum stress ratio is less than 0.40, the total area of T_2 spectrum increases moderately with the increase of maximum stress ratio. When the maximum stress ratio exceeds 0.40, the total area of T_2 spectrum increases dramatically. Fitting analysis reveals that the change of total area increment of T_2 spectrum with maximum stress ratio meets the exponential relation (Eq. (2)), and the correlation coefficient is 0.991 4.

$$\Delta S = 13.159\exp\left(7.412R_{\mathrm{H}}\right) \quad (2)$$

The comparison between the fitting curve and the test results is also given in Fig. 9. It can be also seen that equation (2) can better describe the relationship between the them.

5.2 T_2 spectrum distribution and area under different loading cycles

5.2.1 T_2 spectrum distribution

Figure 10 shows the T_2 spectrum distribution of #7 (R_{H} =0.40) when the number of cycles is 0, 500, 2 000, 5 000, 8 000 and 12 000. As can be seen:

(1) When the number of cycles is 0, 500 and 2 000, the minimum T_2 corresponding to the first T_2 peak of #7 is 0.740 2, 0.280 1 and 0.017 4 ms respectively. When $N \leqslant 2\,000$, as the number of cycles increases, the first T_2 peak gradually moves to the left, indicating that small pores with even smaller size gradually form inside the salt rock. The maximum T_2 corresponding to the last T_2 peak of #7 is 382.749 5, 1 431.458 9 and 2 494.508 1 ms respectively. That is, when $N \leqslant 2\,000$ times, the last T_2 peak moves to the right gradually with increasing number of cycles, indicating that the existing pores in salt rock are gradually connected to form larger pores.

(2) When the number of cycles is 2 000, 5 000, 8 000 and 12 000, the minimum T_2 corresponding to the first T_2 peak of #7 is 0.017 4, 0.024 7, 0.261 3 and 0.369 7 ms respectively. When $N > 2\,000$, the first T_2 peak gradually moves to the right with increasing number of cycles, indicating that the newly generated small pores with smaller aperture in the salt rock gradually form small pores with larger aperture. However, even after 12 000 cycles, the minimum T_2 corresponding to the first peak (0.369 7 ms) of #7 is still smaller than before (0.740 2 ms), implying that after 12 000 cycles, some newly generated pores with smaller aperture is still left in the specimen. The maximum T_2 corresponding to the last peak of #7 is 2 494.508 1, 2 327.202 5, 2 025.501 9 and 2 171.118 0 ms. That is, when $N >$ 2 000, the maximum T_2 corresponding to the last peak basically keep unchanged, reflecting that the maximum aperture of the internal pores of salt rock has reached the maximum after 2 000 cycles under R_{H} =0.40, and then remains nearly constant as the loading cycles increase.

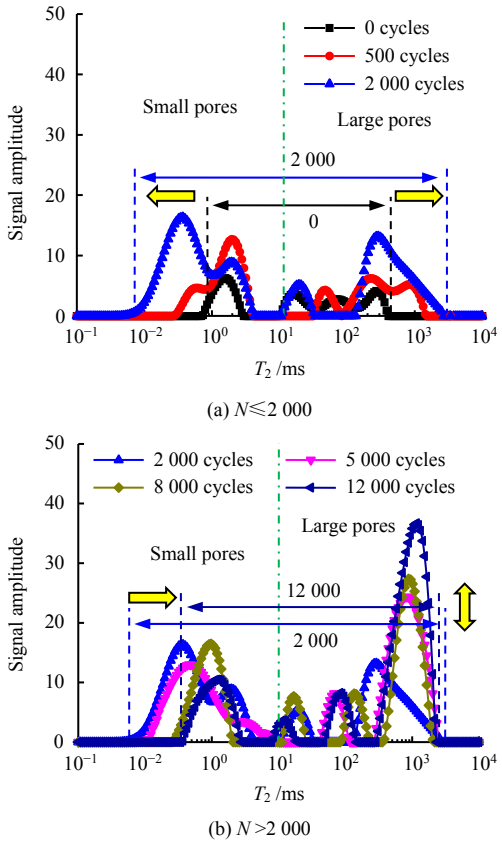

(a) $N \leqslant 2\,000$

(b) $N > 2\,000$

Fig. 10 T_2 spectrum distribution of #7 specimen under different cycle numbers

5.2.2 T_2 spectral area variation

Table 3 lists the T_2 spectral area of specimen #7 subjected to different loading cycles. Fig. 11 illustrates the variation of total T_2 spectral area of #7 and the corresponding areas of large pores and small pores under different cycle numbers. As can be seen from Table 3 and Fig. 11:

(1) The initial pore distribution is dominated by large pores, and the areas of large pores and small pores account for 61.02% and 38.98% of the total T_2 spectral area.

Table 3 Area distribution of T_2 spectrum for specimen #7 under different number of cycles

Cycles	Total area	Small pores		Large pores	
		Area	Proportion /%	Area	Proportion /%
0	203.00	79.13	38.98	123.87	61.02
500	447.12	238.87	53.42	208.25	46.58
2 000	827.08	474.80	57.41	352.28	42.59
5 000	879.77	364.36	41.41	515.42	58.59
8 000	923.82	319.44	39.76	604.38	75.24
12 000	993.55	228.52	23.00	765.03	77.00

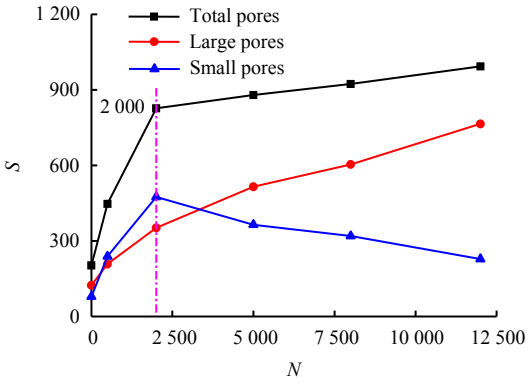

Fig. 11 Variation of total T_2 spectrum area, and the corresponding areas of large pores and small pores for specimen #7 with number of cycles

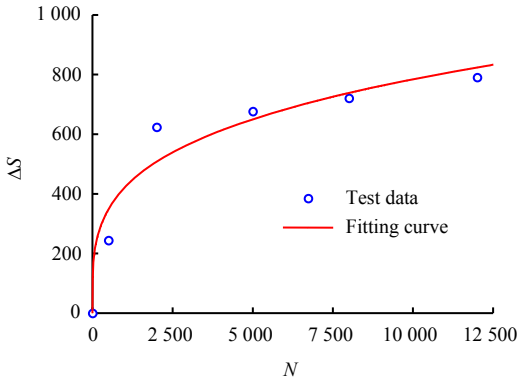

Fig. 12 Variation of total area increment of T_2 spectrum for salt rock with number of cycles

(2) When the number of cycles $N \leqslant 2\ 000$, total pores, large pores and small pores all increase with the increase of N, and the growth rate of small pores is greater than that of large pores. After analysis, when N increases from 0 to 2 000, T_2 spectral areas of total pores, large pores and small pores increase by 624.08, 228.41 and 395.67. After 2 000 cycles, the T_2 areas of large pores and small pores in #7 account for 42.59% and 57.41% of the total area. Compared with the proportions of T_2 area of large pores and small pores to the total area in the initial state (61.02% and 38.98%), when N increases from 0 to 2 000, the proportion of T_2 area of large pores to the total area gradually declines, while that of small pores increases. Therefore, when $N \leqslant 2\ 000$, the change of pore structure in salt rock is characterized by the initiation of small pores.

(3) When the number of cycles $N > 2\ 000$, with the increase of N, total pores and large pores increase continuously, while small pores gradually decrease. From the analysis result, when N increases from 2 000 to 12 000, the total area of T_2 spectrum and corresponding area of large pores increase by 166.47 and 412.75, while the spectral area of small pores decreases by 246.28. Compared with the proportion of the corresponding area of large pores and small pores in the total area in specimen #7 when N=2 000, after N increases from 2 000 to 12 000, the proportion of T_2 area of large pores gradually increases to 77.00%, while that of small pores gradually decreases to 23.00%. Therefore, when $N > 2\ 000$, the pore structure change in salt rock is dominated by the small pores coalescing to formation of large pores.

Figure 12 plots the variation of T_2 spectrum total area increment of #7 with number of cycles. When $N \leqslant 2\ 000$, the total area increment of T_2 spectrum increases rapidly. When $N > 2\ 000$, the total area increment still increases at a lower increase rate.

By fitting analysis, the variation of T_2 spectrum total area increment of #7 with number of cycles can be well expressed using Eq. (3), and the correlation coefficient R=0.972 8. It can be seen in Fig.3 that Eq.(3) fits the test data well.

$$\Delta S = 65.01N^{0.27} \tag{3}$$

6 Empirical fatigue model

6.1 Modeling

According to the existing rock fatigue constitutive models, although the damage models are able to describe the fatigue deformation of rock under cyclic loading, it is difficult to choose appropriate damage variables to represent the damage evolution. The fatigue constitutive models based on element combined model theory possess the disadvantages of complex form and many undetermined parameters. Meanwhile, the application of this method to describe the irreversible deformation of rock needs to artificially divide the original fatigue deformation into three stages, and different functions are required to describe the deformation law in all stages, which cannot be expressed by a unified function.

As can be seen from Fig. 5, when the maximum stress ratio R_H is 0.74 and 0.85, specimen #5 and #6 are damaged during the test. The change of cumulative irreversible deformation can be divided into initial, constant rate and accelerated stages, as represented in curve 1 in Fig. 13. If a symmetric curve of curve 1 is drawn along the line $\varepsilon = N$, curve 2 is obtained. Since the equations of the two curves are inverse functions of each other, as long as the equation of curve 2 is determined, the equation of curve 1, namely the fatigue constitutive equation of salt rock, can be obtained.

Curve 2 belongs to S-shaped growth curve, and its equation can be expressed by MMF function, Logistic function, Gompertz function and Weibull function. Among them, MMF function is widely used, and expressed as [32]

$$y = \frac{ax^b}{m + x^b} \tag{4}$$

where x and y are independent variable and dependent variable; a, b and m are material constants (b>1), and a represents the maximum value of the dependent variable.

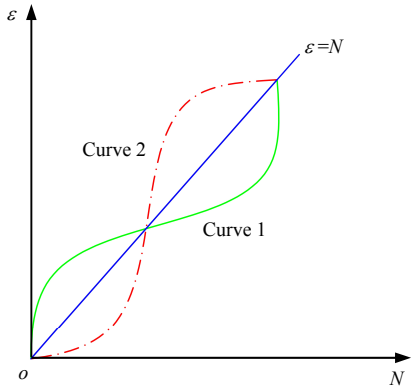

Fig. 13 Sketch map for the inverse function of the cumulative irreversible deformation curve

The inverse function of Eq. (4) is calculated as

$$x=\left(\frac{ym}{a-y}\right)^{\frac{1}{b}} \tag{5}$$

In the cumulative irreversible deformation curve, independent variable x and dependent variable y are loading cycle numbers N and cumulative irreversible deformation ε respectively. Replace x and y in Eq. (5) with ε and N, then

$$\varepsilon=\left(\frac{Nm}{a-N}\right)^{\frac{1}{b}} \tag{6}$$

In Eq. (4), a denotes the maximum value of dependent variable y, and thus a in Eq. (6) represents the maximum of number cycles N, namely, the rock fatigue life N_{F}. In addition, for simplifying expression, let $1/b=n$ in Eq. (6), then Eq. (6) is transformed into

$$\varepsilon=\left(\frac{m\dfrac{N}{N_{\mathrm{F}}}}{1-\dfrac{N}{N_{\mathrm{F}}}}\right)^{n} \tag{7}$$

It should be noted that b>1 in Eq. (4), so in Eq. (7), n<1.

Pan et al. pointed out that the relationship between material fatigue life and maximum/minimum cycling stress of cyclic loading is as follows [33]:

$$N_{\mathrm{F}}=\frac{1}{p}\left[\sigma_{\max}\left(\frac{\sigma_{\max}-\sigma_{\min}}{2}\right)\right]^{-q}=\frac{1}{p}\left(\sigma_{\max}\sigma_{\mathrm{a}}\right)^{-q} \tag{8}$$

where p and q are underdetermined parameters.

Substitute Eq. (8) into Eq. (7) yields

$$\varepsilon=\left[\frac{mpN\left(\sigma_{\max}\sigma_{\mathrm{a}}\right)^{q}}{1-pN\left(\sigma_{\max}\sigma_{\mathrm{a}}\right)^{q}}\right]^{n} \tag{9}$$

Eq. (9) is the final expression of rock fatigue model obtained by solving the inverse of S-shaped function.

6.2 Parameters determination

According to Eq. (9), there are four undetermined parameters (p, q, m and n).

Among them, p and q can be determined according to the fatigue life under two-stage loads. Assuming that when the maximum cycling stress is σ_{c} and σ_{d}, and the minimum cycling stress is σ_{cl} and σ_{dl}, the corresponding fatigue life is N_{Fc} and N_{Fd}. Substituting (σ_{c}, σ_{cl}, N_{Fc}) and (σ_{d}, σ_{dl}, N_{Fd}) into Eq. (8), a binary linear system of equations is established, and then the values of c and d can be obtained.

Parameters m and n can be determined by fitting the fatigue test results. The operation procedure is as follows:

(1) Consider parameters m and n as the design variables P:

$$P=\left(m,n\right) \tag{10}$$

(2) Establish objective function Y:

$$Y=\sum_{j=1}^{J}\left[\lambda_{\mathrm{j}}\left(P,t_{\mathrm{j}}\right)-\lambda_{\mathrm{j}}\right]^{2} \tag{11}$$

where J is the number of test groups; $\lambda_{\mathrm{j}}\left(P,t_{\mathrm{j}}\right)$ and λ_{j} are the calculated value and measured value of deformation at time t_{j}.

(3) Set the control precision of the objective function, and then solve it iteratively. After the objective function meets the accuracy requirements, the iteration is stopped and the results are output.

6.3 Model validation

The fatigue test results of salt rock are used to verify the rationality of the proposed model. The model parameters are determined according to the method introduced in Section 6.2, as listed in Table 4.

Table 4 Determination results of model parameters

Specimen	Maximum cycling stress /MPa	Minimum cycling stress /MPa	Parameters			
			p	q	m	n
#1	8	5	4.449×10^{-13}	3.552	1.367×10^{-48}	0.045
#2	14	5			4.554×10^{-31}	0.064
#3	20	5			7.593×10^{-23}	0.079
#4	23	5			8.870×10^{-20}	0.087
#5	26	5			3.869×10^{-17}	0.091
#6	30	5			4.157×10^{-14}	0.108

Table 4 suggests that parameters m and n are constantly changing with the maximum cycling stress. Meanwhile, as the stress amplitude of cyclic loading $\sigma_{\mathrm{a}}=(\sigma_{\max}-\sigma_{\min})/2$, m and n are necessarily related to function $f(\sigma)=\sigma_{\max}\sigma_{\mathrm{a}}$ in Eqs. (8) and (9). Therefore,

if the quantitative relationship between m, n and $f(\sigma)$ can be established, it is of crucial value to predict the cumulative irreversible deformation of salt rock under arbitrary maximum/minimum cycling stress.

The analysis reveals that the relationship between $-\lg m$, n and $f(\sigma)$ can be described by the function expressed by Eqs. (12) and (13), and the correlation coefficient R is 0.999 4 and 0.996 1. Fig. 14 compares the fitting curve with the parameters inversion results in Table 4. It is clear that Eqs. (12) and (13) reflect the changing law of $-\lg m$, n with $f(\sigma)$ very well.

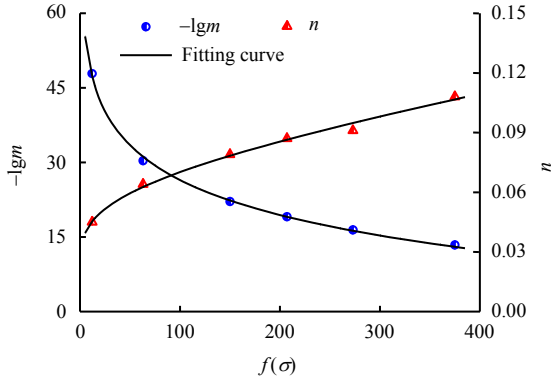

Fig. 14 Variation of parameters *m* and *n* with *f*(σ)

$$-\lg m = -10.226\ln\left[f(\sigma)+1\right]+76.644 \quad (12)$$

$$n = \frac{1}{4\,518.320 - 4\,487.068 f(\sigma)^{8.206\times10^{-4}}} \quad (13)$$

By substituting p=4.449×10^{-13}, q=3.552, Eqs. (12) and (13) into Eq. (9), the cumulative irreversible deformation prediction curves of salt rock under different R_H can be obtained. The comparison between the prediction curves and test results are presented in Fig. 15. The proposed fatigue model can not only describe the initial and constant rate stages of cumulative irreversible deformation of salt rock under a lower R_H (#1 to #4), but also describe the accelerated stage under a higher R_H (5# and 6#).

In terms of the degree of coincidence, there is certain error when R_H is 0.74 and 0.85. For other R_H, the test results are in good consistence with the predicted curves. In general, this model is able to describe the variation of cumulated irreversible deformation of salt rock with numbers of cycles under different R_H. Meanwhile, it can be seen from Eq. (9) that the new model involves less parameters (only four parameters), and the expression is simple and convenient for application.

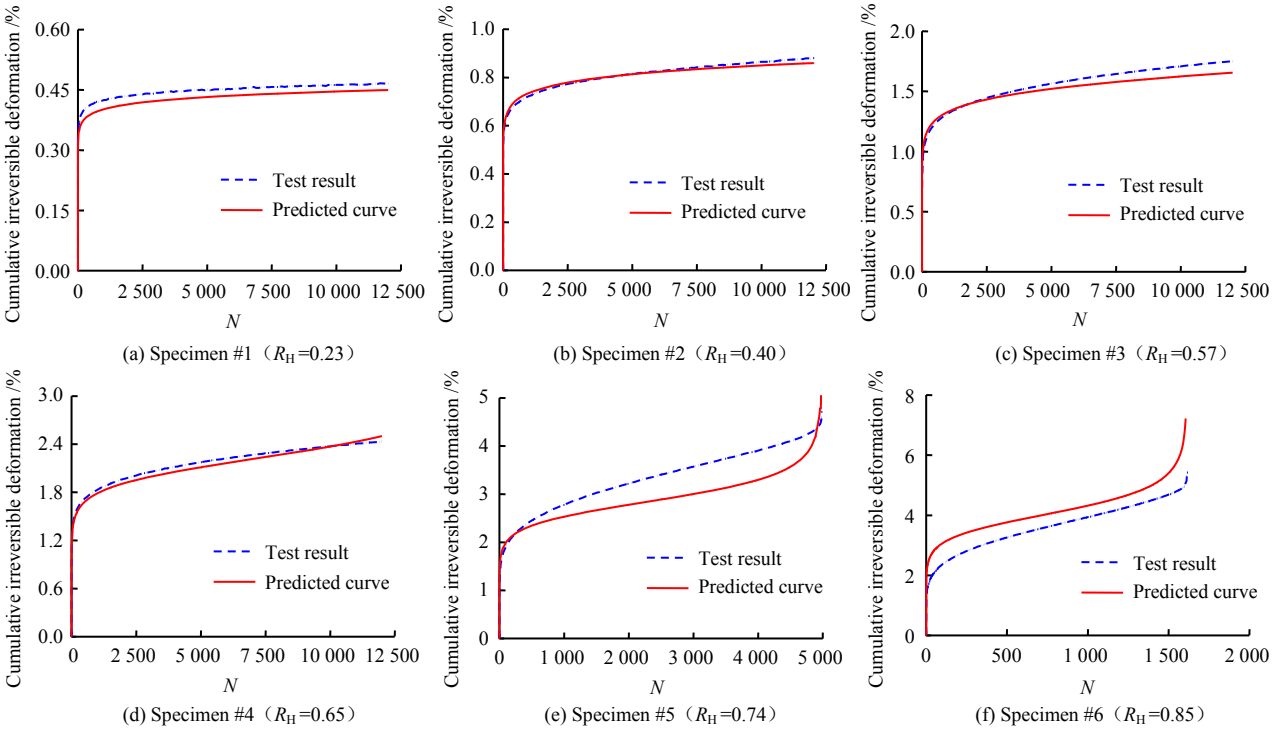

Fig. 15 Comparison between predicted curves and test data

7 Discussion

7.1 Applicability of the fatigue model

Numerous studies have proved that there is a fatigue failure threshold for rock under cyclic loading [34]. When the maximum cycling stress is lower than the threshold, cumulative irreversible deformation will reach the maximum cycling stress with increasing number of cycles, and remain stable after that. In this case, rock does not undergo fatigue failure. When the maximum cycling stress exceeds the threshold, cumulative irreversible deformation will continue to increase with

the increase of number of cycles until the fatigue failure occurs. For the proposed model, according to Eq. (9), even if the maximum cycling stress is low, the cumulative irreversible deformation will increase with number of cycles, and fatigue failure will eventually occur. As a consequence, the model proposed cannot describe the irreversible deformation of rock under the condition that the maximum cycling stress is lower than the fatigue failure threshold.

Ma et al.[6], Guo et al.[7] stated that the ratio of fatigue failure threshold to uniaxial compressive strength of salt rock is about 0.8. However, for the salt rock specimens used in this study, even if the maximum stress ratio is only 0.23, after 12 000 cycles the cumulative irreversible deformation does not reach the maximum yet, but presents a slow upward trend with increasing number of cycles (Fig. 16), which is consistent with the case reflected by our model.

In the meantime, salt cavern CAES station usually only experiences one gas injection and recovery cycle a day. Accordingly, the number of cycles experienced by the surrounding rock in its designed service life (30 a) is about 11 000. For fatigue model proposed, when the maximum and minimum stress ratios are 0.23 and 0.14 respectively, although fatigue failure will occur, the fatigue life reaches 3.296×10^8 times (Eq. (8)), which is far greater than the number of cycles (11 000) experienced by the surrounding rock in the designed service life. Hence, when the maximum cycling stress is low, it can be considered that the fatigue life of salt rock is infinite, indicating the fatigue failure will not occur during the production of a salt cavern CAES station.

In conclusion, it is feasible to use the model proposed to describe the irreversible deformation law of salt rock when the maximum cycling stress is lower than the fatigue failure threshold.

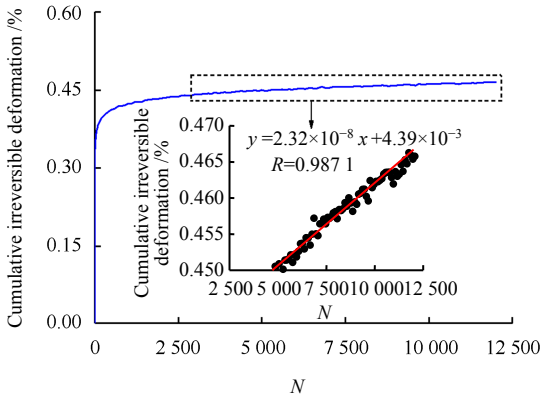

Fig. 16 Variation of cumulative irreversible deformation of specimen #1 with number of cycles

7.2 Shortcomings

For salt cavern gas storage, it commonly only experiences 1−2 gas injection and recovery cycles a year, while salt cavern CAES station usually experiences one gas injection and recovery cycle a day. In engineering practice, it takes a long time for the internal pressure in the gas storage to increase from the minimum operating pressure to the maximum, or decrease from the maximum operating pressure to the minimum. The rate and frequency of cyclic loading and unloading on surrounding rock are relative lower. At such low frequencies, both fatigue deformation and creep deformation will happen in the surrounding rock. Predictably, the deformation process is extremely complicated by the coupling of creep and fatigue.

In this paper, the cyclic loading frequency is set as 1 Hz to study the fatigue properties of salt rock, meaning that the axial stress increasing from the minimum cycling stress to the maximum, or decreasing from the maximum cycling stress to the minimum only lasts for 0.5 s. Under this condition, the stress acting on salt rock changes significantly, and the maximum change rate can reach up to 50 MPa/s. Due to the high loading cycling frequency and short test period, the creep deformation of salt rock is very small and negligible. Therefore, the cyclic loading and unloading test with a frequency of 1 Hz can be regarded as a pure fatigue test. Due to the difference of loading frequency, there is a certain gap between our test results and engineering experiences, more comparisons are warranted to ascertain the specific discrepancy. Therefore, the mechanical properties of salt rock under low-frequency cyclic loading (considering the coupling effects of fatigue and creep) need to be further examined in the following research.

8 Conclusions

(1) Under cyclic loading, intergranular cracks are the main propagation mode of cracks in salt rock, and the number of cracks increases with the increase of maximum stress ratio. In addition, fatigue failure occurs in salt rock, and a handful of intragranular cracks and transgranular cracks also appear when the maximum stress ratio is 0.74 and 0.85.

(2) When the maximum stress ratio is 0.23 and 0.40, the minimum pore size decreases and the maximum pore size increases after 12 000 cycles. When the maximum stress ratio is 0.57 and 0.65, the minimum pore size and maximum pore size increase. After the fatigue test, the number of large pores and total pores in salt rock goes up, while the number of small pores declines. For large pores, small pores and

total pores, the increase of maximum stress ratio will aggravate their inherent trends.

(3) When the maximum stress ratio is 0.40 and the number of cycles increases from 0 to 2 000, the minimum pore size of the inner pores decreases gradually, whereas the maximum pore size increases. Meanwhile, the quantities of small pores, large pores and total pores in salt rock all increase with number of cycles. However, the growth rate of small pores is more prominent than that of large pores, and the formation of small pores dominates the pore structure change in salt rock.

(4) When the maximum stress ratio is 0.40 and the number of cycles increases from 2 000 to 12 000, the minimum pore size increases continuously, while the maximum pore size is basically unchanged, indicating that the maximum pore size has reached the peak after 2 000 cycles. Moreover, the numbers of large pores and total pores increase with number of cycles, but the number of small pores decreases, proving that the formation of large pores is the main change of pore structure.

(5) An empirical fatigue model with less parameters and simple form is established by solving the inverse function of S-shaped function, and the rationality is verified by our test results. The results show that the model can accurately characterize the variation of cumulative irreversible deformation of salt rock with number of cycles under different maximum cycling stresses.

Although the variation of pore quantity and radius with number of cycles and maximum cycling stress during fatigue deformation has been obtained through experiments, it should be noted that conclusions (1)−(4) were drawn based on the site-specific specimens. Considering the diversity of rock categories and complexity of rock minerals composition and mechanical properties, whether these conclusions are universally applicable to other rocks or salt rocks from other regions remains to be verified experimentally. Finally, the empirical fatigue model proposed in this paper is established from the point of macroscopic phenomenology. The theoretical curve of the model conforms to the three-stage variation of rock fatigue deformation, so it can be applied to describe the irreversible deformation of other rocks or salt rocks from other regions.

References

[1] WANG J B, ZHANG Q, SONG Z P, et al. Creep properties and damage constitutive model of salt rock under uniaxial compression[J]. International Journal of Damage Mechanics, 2020, 29(6): 902−922.

[2] LIANG Wei-guo, CAO Meng-tao, YANG Xiao-qin, et al. Experimental study on creep of glauberite salt rock under coupled compression and dissolution[J]. Chinese Journal of Rock Mechanics and Engineering, 2016, 35(12): 2462−2470.

[3] JI Wen-dong, YANG Chun-he, YAO Yuan-feng, et al. Effects of loading strain rate on mechanical performances of salt rock[J]. Chinese Journal of Rock Mechanics and Engineering, 2011, 30(12): 2507−2513.

[4] XU Hong-fa, WANG Chen, MA Lin-jian, et al. Volumetric strain of rock salt under triaxial low-frequency cyclic loading[J]. Chinese Journal of Geotechnical Engineering, 2015, 37(4): 741−746.

[5] WANG J B, ZHANG Q, SONG Z P, et al. Experimental study on creep properties of salt rock under long-period cyclic loading[J]. International journal of Fatigue, 2021, 143: 106009.

[6] MA Lin-jian, LIU Xin-yu, XU Hong-fa, et al. Deformation and strength properties of rock salt subjected to triaxial compression with cyclic loading[J]. Chinese Journal of Rock Mechanics and Engineering, 2013, 32(4): 849−856.

[7] GUO Yin-tong, ZHAO Ke-lie, SUN Guan-hua, et al. Experimental study of fatigue deformation and damage characteristics of salt rock under cyclic loading[J]. Rock and Soil Mechanics, 2011, 32(5): 1353−1359.

[8] REN Song, BAI Yue-ming, JIANG De-yi, et al. Experimental study of temperature effect on fatigue property of salt rock[J]. Chinese Journal of Rock Mechanics and Engineering, 2012, 31(9): 1839−1845.

[9] POUYA A, ZHU C, ARSON C. Micro-macro approach of salt viscous fatigue under cyclic loading[J]. Mechanics of Materials, 2016, 93: 13−31.

[10] FAN J Y, CHEN J, JIANG D Y, et al. Fatigue properties of rock salt subjected to interval pressure[J]. International Journal of Fatigue, 2016, 90: 109−115.

[11] JIANG De-yi, FAN Jin-yang, CHEN Jie, et al. Influence of interval fatigue tests on fatigue characteristics of salt rock[J]. Chinese Journal of Geotechnical Engineering, 2016, 38(7): 1181−1186.

[12] PENG H H, FAN J Y, ZHANG X, et al. Computed tomography analysis on cyclic fatigue and damage properties of rock salt under gas pressure[J]. International Journal of Fatigue, 2020, 134: 105523.

[13] CHEN Jian-wen, YANG Chun-he. Mesoscopic deformation based plastic constitutive model of salt rock[J]. Rock and

Soil Mechanics, 2015, 36(1): 117−122.

[14] LI Hao-ran, YANG Chun-he, LIU Yu-gang, et al. Experimental study of ultrasonic velocity and acoustics emission properties of salt rock under uniaxial compression load[J]. Chinese Journal of Rock Mechanics and Engineering, 2014, 33(10): 2107−2116.

[15] LI Shu-chun, XU Jiang, TAO Yun-qi, et al. Low cycle fatigue damage model and damage variable expression of rock[J]. Rock and Soil Mechanics, 2009, 30(6): 1611−1614, 1619.

[16] WANG Y S, MA L J, FAN P X, et al. A fatigue damage model for rock salt considering the effects of loading frequency and amplitude[J]. International Journal of Mining Science and Technology, 2016, 26(5): 955−958.

[17] LI T T, PEI X J, WANG D P, et al. Nonlinear behavior and damage model for fractured rock under cyclic loading based on energy dissipation principle[J]. Engineering Fracture Mechanics, 2019, 206: 330−341.

[18] LIU X S, NING J G, TAN Y L, et al. Damage constitutive model based on energy dissipation for intact rock subjected to cyclic loading[J]. International Journal of Rock Mechanics and Mining Sciences, 2016, 85: 27−32.

[19] XIAO J Q, DENG J Q, JIANG F L, et al. Fatigue damage variable and evolution of rock subjected to cyclic loading[J]. International Journal of Rock Mechanics and Mining Sciences, 2009, 47(3): 461−468.

[20] GUO Jian-qiang, HUANG Zhi-hong. Constitutive model for fatigue of rock under cyclic loading[J]. Chinese Journal of Geotechnical Engineering, 2015, 37(9): 1698−1704.

[21] PENG Shu-quan, WANG Pei-yu, FAN Ling, et al. Research on elasto-plastic viscous fatigue constitutive model of jointed rock[J]. Rock and Soil Mechanics, 2021, 42(2): 379−387.

[22] LI Yong-hui, PU Shao-yun, RAO Jun-ying, et al. Study on a modified Nishihara fatigue model for rock with cyclic loading[J]. Water Resources and Hydropower Engineering, 2017, 48(7): 129−135.

[23] TANG Xin, YU Jin, LIN Li-hua, et al. Equivalent fatigue stress and non-linear constitutive model for fatigue of rock[J]. Chinese Journal of Geotechnical Engineering, 2021, 43(3): 102−111.

[24] LIU J H, PU S Y, RAO J Y. Visco-elastoplastic constitutive fatigue model for rocks[J]. Advances in Civil Engineering, 2020(1): 4292043.

[25] WANG Jun-bao, LIU Xin-rong, SONG Zhan-ping, et al. A whole process creeping model of salt rock under uniaxial compression based on inverse S function[J]. Chinese Journal of Rock Mechanics and Engineering, 2018, 37(11): 2446−2459.

[26] CAI Mei-feng, HE Man-chao, LIU Dong-yan. Rock mechanics and engineering[M]. Beijing: Science Press, 2002.

[27] ZHANG Gui-min, WANG Zhen-shuo, LIU Yu-xuan, et al. Research on stability of the key roof above horizontal salt cavern for compressed air energy storage[J]. Rock and Soil Mechanics, 2021, 42(3): 800−812.

[28] ZHAO Ke-lie. Research on the usability of underground salt rock gas storage in the process of gas injection and production[D]. Wuhan: Institute of Rock and Soil Mechanics, Chinese Academy of Sciences, 2009.

[29] WANG J B, ZHANG Q, SONG Z P, et al. Mechanical properties and damage constitutive model for uniaxial compression of salt rock at different loading rates[J]. International Journal of Damage Mechanics, 2021, 30(5): 739−763.

[30] TANG Z Q, ZHAI C, ZOU Q L, et al. Changes to coal pores and fracture development by ultrasonic wave excitation using nuclear magnetic resonance[J]. Fuel, 2016, 186: 571−578.

[31] YANG X Y, WENG L, HU Z X. Damage evolution of rocks under triaxial compressions: an NMR investigation[J]. KSCE Journal of Civil Engineering, 2018, 22(8): 2856−2863.

[32] WANG Jun-bao, LIU Xin-rong, LI Peng, et al. Study on prediction of surface subsidence in mined-out region with the MMF model[J]. Journal of China Coal Society, 2012, 7(3): 411−415.

[33] PAN Hua, QIU Hong-xing. Fatigue model of concrete based on continuum damage mechanics[J]. Journal of Southeast University (Natural Science Edition), 2006, 36(4): 605−608.

[34] GE Xiu-run. Study on deformation and strength behavior of the large-sized triaxial rock samples under cyclic loading[J]. Rock and Soil Mechanics, 1987, 8(2): 11−19.